Isolating the impacts of urban form and fabric from geography in assessing heat mitigation strategies

Kerry A. Nice[a,*], Negin Nazarian[b,c], Mathew J. Lipson[b], Melissa A. Hart[b], Sachith Seneviratne[a], Jason Thompson[a], Marzie Naserikia[b], Branislava Godic[a], Mark Stevenson[a,d]

[a]*Transport, Health, and Urban Design Research Lab, Faculty of Architecture, Building, and Planning, University of Melbourne, VIC, Australia.*
[b]*ARC Centre of Excellence for Climate Extremes, University of New South Wales, Sydney, NSW, Australia.*
[c]*School of Built Environment; and City Futures Research Centre, University of New South Wales, Sydney, NSW, Australia.*
[d]*Melbourne School of Engineering; and Melbourne School of Population and Global Health, University of Melbourne, VIC, Australia.*

Abstract

As public health risks resulting from urban heat in cities increase due to urbanisation and climate change, there is a pressing need to design strategies for urban heat mitigation and ensure that future development is climate sensitive. Heat stress in cities is mainly influenced by four factors: the built form, natural and vegetated form, human urban activities, and regional geographic settings (e.g. topography and distance to water bodies). The first two factors can be modified and redesigned as urban heat mitigation strategies (e.g. changing the albedo of surfaces, replacing hard surfaces with pervious vegetated surfaces, or increasing canopy cover), whereas while human activities can be modified, the impacts of these can be difficult to quantify, and regional geographical settings of cities cannot be modified. However, when evaluating the effectiveness of urban heat mitigation strategies based on modifications to the built and natural forms, it can be difficult to separate their impacts from the interactions of the geographic influences. To address this, we performed a comprehensive urban form analysis, covering the full range of realistic built and natural forms (building density and height, roads, grass, and tree density and height) in cities, along with a combination of mitigation strategies, to determine the importance and influence of each on thermal performance. We show that during the daytime, higher air temperatures and Universal Thermal Climate Index temperatures are strongly driven by increased street fractions, with air temperatures increasing up to 10 and 15°C as street fractions increase to 80 and 90%. Reductions in air temperature of 5°C are seen with increasing grass and tree fractions from none to complete coverage. Similar patterns are seen with the Universal Thermal Climate Index, with increasing street fractions of 80% and 90% driving increases of 6 and 12°C. We then scale up the results to produce city-wide heat maps of several Australian cities showing the impact of present day urban form. The resulting method allows mitigation strategies to be tested on modifiable urban form factors isolated from geography, topography, and local weather conditions, factors that cannot easily be modified.

Keywords: micro-climate modelling, urban morphology, heat mitigation, urban heat

1. Introduction

1.1. Need for urban heat mitigation measures

Measures of cumulative heat show significant increases in recent decades with trends of increased heatwave frequency and duration seen globally (Perkins-Kirkpatrick and Lewis, 2020). Exposure to dangerous levels of heat stress are expected to increase by a factor of 5-10 by 2080 (Coffel et al., 2018), driven by more frequent, severe, and long-lasting heatwaves (IPCC, 2013). Heat in urban areas is the most dangerous natural hazard in Australia (Coates et al., 2014), with disproportionate risks falling on vulnerable populations such as elderly and the very young (Nicholls

*Principal corresponding author
Email address: kerry.nice@unimelb.edu.au (Kerry A. Nice)

et al., 2008). The design of cities has enhanced these risks by replacing natural pervious land covers with hard heat absorbent surfaces, resulting in increased heat stress for inhabitants (Coutts et al., 2012; Martilli et al., 2020). This urbanisation of land-use has altered the urban energy balance (Oke, 1982). Anthropogenic waste heat from buildings and transport and reduced shading through diminishing tree canopy cover result in larger amounts of net energy at street level. Meanwhile, the conversion of vegetated to impervious surfaces, and the reduction of available water in cities, shifts the urban energy balance away from latent heat (water evaporation) towards increased sensible heat (heat that can be felt) and increased heat storage in urban surfaces.

Mitigation strategies that incorporate findings from urban climate research into planning of future developments can ensure that newly built areas are climate sensitive and better able to address the adverse effects of urban design on the thermal environment. These strategies, which rely on modifications to built form, fabric, and natural land cover in cities, require both an understanding of the processes driving excess heat, and the methods required to identify the existing areas of high risk that will benefit most from interventions. Krayenhoff et al. (2021), in a systematic review, identified commonly used urban heat mitigation strategies, including cooling through albedo changes, vegetation cover, irrigation and water, and photovoltaic panels. Albedo changes, increasing the reflectivity of urban surfaces, can reduce road and sidewalk surface temperatures but may cause increased radiant loads for pedestrians (Middel et al., 2020). If applied at roof levels, albedo changes can provide urban heat reductions (Jacobs et al., 2018). Urban vegetation provides cooling benefits through shading of urban surfaces and evapotranspiration (Bowler et al., 2010; Coutts et al., 2012, 2015), as well as reducing hard impervious surfaces in favour of pervious vegetated surfaces (Middel and Krayenhoff, 2019). Additional cooling can also be realised through irrigation of both vegetated (Broadbent et al., 2017; Cheung et al., 2021) and impervious surfaces (Hendel et al., 2016; Solcerova et al., 2018).

In a review of the influence of cities on local meteorology, Masson et al. (2020b) found that urban climates and heat stress in cities are influenced by four main factors, 1) the built form, 2) the natural and vegetated form (i.e. soil, water, vegetation and their phenology), 3) urban functions (heat released by human activities), and 4) regional geographic settings. As noted above, (1) and (2) are often the focus of mitigation strategies. However, the interaction of the different elements of urban form as well as the compounding effect on canopy temperatures and heat stress are often non-linear. The complexity of these interactions makes quantifying the impact of each mitigation measure difficult across different cities and their individual mixes of urban form. Additionally, each city's regional geography (including topography and distance from and orientation to an ocean) adds additional complexity in separating the impact of mitigation measures from the geography influence.

1.2. Metrics to assess urban heat mitigation measures

Assessing the effectiveness of cooling strategies requires metrics to measure urban heat. These metrics need to account for different scales and be carefully chosen for the intended purpose. Scales used to assess urban climates are commonly defined (Oke et al., 2017) at a mesoscale (10km and greater), a micro-scale which provides an 'in-street' climate (under 1km), and an overlapping local scale between the two (100m to tens of kms). Air temperatures will show the least variability in nearby locations across a neighbourhood or precinct, for example, Coutts et al. (2015) finds air temperature differences of approximately 1.5°C between two adjoining identical street canyons varying only by the level of canopy cover (an open canopy vs. much more extensive tree cover). Air temperatures can be measured using simple equipment, however more extensive observations of variability across a local area require a dense network of instruments (Potgieter et al., 2021), as well as additional information to untangle the local weather conditions or topography from the influence of the urban form.

Surface temperatures, on the other hand, can show wide ranges in variability across a micro-scale depending on the surface types and whether the surfaces are shaded or not. Surface temperatures of shaded surfaces will be similar to the surrounding air temperatures while nearby unshaded surfaces can be 20-30°C hotter. Land surface temperature (LST) can be remotely sensed using satellite or aircraft, quickly mapping wide areas, but observations are limited to the fly-over time. LST has often been used to identify hotspots (Aniello et al., 1995) or to evaluate cooling strategies (Zhu et al., 2012; Duncan et al., 2018; Manoli et al., 2019; Ossola et al., 2021), however the validity of these results and the ability to link LST, which is measured at the top of the urban canopy, to thermal comfort at ground level can be limited and misleading (Coutts et al., 2016). As the shading provided by the urban canopy (both vegetation and urban structures) is a significant cooling mechanism (Coutts et al., 2015; Lee et al., 2018; Krayenhoff et al., 2021), these effects will not be captured in an above-canopy assessment. Obtaining under-canopy surface temperature observations of these heterogeneous environments is challenging, time consuming and limited in scale

and resolution and to the observation time period (Middel and Krayenhoff, 2019). To capture all of the influences of urban geometry and materials on human thermal comfort, especially the influence on mean radiant temperature (Kántor and Unger, 2011) (a temperature that accounts for the thermal stresses on a person from both solar exposure and energy/heat radiating from nearby surfaces), requires micro-scale observations and specialised equipment. This can also be seen when calculating human thermal comfort (HTC) indexes, such as the Universal Thermal Climate Index (UTCI) (Bröde et al., 2012), which provides equivalent temperatures of heat stress, as they too incorporate all of these types of temperatures (and require observations of each).

1.3. Modelling urban heat mitigation measures

Modelling can be of use in assessing thermal impacts across different urban arrangements and compositions and can provide the full range of temperature metrics (including air temperature and UTCI) at different temporal and spatial resolutions. Masson et al. (2020a) identifies the two main requirements for useful urban climate modelling; appropriate modelling scale and availability of descriptive data of urban areas. Resolving urban areas requires at least mesoscale modelling, with the urban features often represented as simplified and idealised (e.g., 2-dimensional) versions of the urban 3D geometry (Masson, 2005). This scale can be used to assess strategies with large scale impacts on parameters with low variability such as above roof air temperature. The necessary urban morphology and land cover data for this scale of analysis can be supplied through databases such as the World Urban Database and Access Portal Tools (WUDAPT) project (Ching et al., 2018). This project has been building an open access database of all the world's urban areas. Their initial efforts focused on building maps of local climate zones (LCZ) (Stewart and Oke, 2012), a standardised classification system to describe urban morphology typologies, and provides local-scaled resolution coverage of wide areas of the world (Demuzere et al., 2019).

Human thermal comfort modelling of urban areas needs to be undertaken in 3-dimensions at a micro-scale resolution, thereby accounting for the influence of shading, vegetation, and water features. Examples of models at this scale that account for vegetation impacts and urban hydrology, or that can explicitly calculate parameters needed to estimate human thermal comfort, include: ENVI-met (Bruse, 1999), VTUF-3D (Nice et al., 2018), SOLWEIG/UMEP (Lindberg et al., 2018), PALM (Dominik and Andreas, 2019), canyon air temperature (CAT) (Erell and Williamson, 2006), and OTC3D (Nazarian et al., 2018).

While WUDAPT datasets are currently of insufficient resolution to support micro-scaled modelling, a pathway has been planned (Ching et al., 2019) using satellite imagery and Open Street Map to refine the land cover resolution to 2m and provide a complete set of urban canopy parameters needed for modelling, including building heights and footprints, and catalogues of urban form typologies (material types and properties, vegetation types, and building ages). Other sources of urban information are also becoming available, such as the commercial provider Geoscape (Geoscape, 2020), which provides 2m resolution land cover coverage, as well as building and tree heights and footprints, of major Australian cities. However, an open dataset with world-wide coverage at a scale sufficient for micro-scaled modelling does not currently exist.

1.4. Comprehensive urban form analysis to inform urban heat mitigation strategies

A comprehensive set of sensitivity analyses covering the full range of realistic built and natural forms in cities, combined a range of mitigation strategies, can be used to isolate the influence of the city form from the geography. Previously, analyses such as these have been limited to a class-based assessment to provide the urban form input for climate modelling of specific areas (Stewart et al., 2014; Verdonck et al., 2018; Hammerberg et al., 2018; Masson et al., 2020a; Emery et al., 2021) or using remote sensed LST (Alexander, 2021; Li et al., 2022; Peng et al., 2022) or low resolution air temperatures observations (Potgieter et al., 2021). However, urban morphology parameter ranges for classes can be quite broad. For example, for the LCZ6 class (the open low-rise typology), impervious surface fractions can range from 20-50% and pervious of 30-60%. However, as the results of this study will show, significant differences in thermal outcomes can be seen across these ranges. In addition, the difficulty in linking remote sensed LST to ground level thermal comfort has been noted above.

VTUF-3D is a surface energy balance micro-climate model that accounts for the distribution of radiative fluxes between surfaces in an explicit 3-dimensional urban canyon representation, and can also account for the impacts of vegetation shading and evapotranspiration. It produces high-resolution predictions of surface temperatures, mean radiant temperature, and UTCI. This study will generate a comprehensive set of thousands of possible urban form

combinations and individually model each of those using VTUF-3D. This will quantify both the relative influence of each surface type in the urban mix and the sensitivity of canopy temperatures and UTCI to a combination of design parameters. As an application example, the results from each combination of urban form and fabric will be applied back to individual locations, as determined by high resolution Geoscape data, to provide a micro-scaled thermal comfort map of a large urban area. This approach allows the isolation of the effects of local urban form from influences present in larger-scale modelling, such as regional climate, topography, and coastal breezes.

Therefore, in this study we introduce a method that determines the influence of *just* urban form on thermal comfort, by utilising a comprehensive combination of possible urban forms, an urban morphology data source, and micro-climate modelling. This is then applied at a city-wide scale to identify areas that may benefit from heat mitigation interventions, and to inform planning and development of new climate sensitive urban form. The first objective will be to model the full range of representative combinations of urban form (mixes of land cover and urban and vegetative structure) at a micro-scale. The second objective will be to use these results to determine the importance and relative influence of each feature type on thermal performance. The final objective will be to build the results back up to a city-wide assessment of thermal comfort generated by urban form.

2. Methods

The overall workflow for this project is presented in Figure 1. Each step is detailed in the following sections.

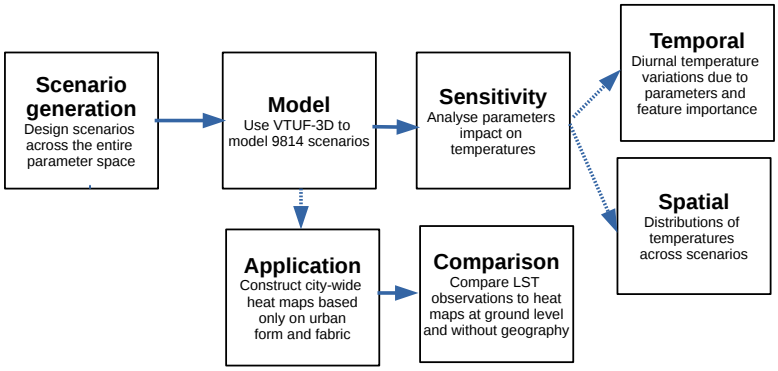

Figure 1: **Workflow flow for this project.**

2.1. Scenario generation

Modelling domains of 100×100m of 5m resolutions were created by iterating through all fractions (in 5% increments) of trees, grass, buildings and streets, as well as heights (in 0.5m increments) of buildings (from 0 to 49 meters) and vegetation (from 0 to 20 meters) (Figure 2). For example, a single domain might consist of 20% buildings, 30% grass, 30% streets, and 20% trees and the average building height (across the entire domain) of 4.5m and average tree height of 3.0m and multiple variations as building heights are iterated from 0m to 49m and trees from 0m to 20m. This resulted in 9814 scenarios. Note, the distribution of surface types were intended to resemble an urban canyon unit starting with a road through the middle and other types distributed on either side. See Supplementary Figure S5 showing the distribution of surface fractions across all the modelled domains. Heights of individual buildings and trees could reach the maximum heights but heights and locations were weighted to achieve a specific sky view factor (as related to average domain heights). Average heights can be calculated in two different ways. For example, in the scenario in Figure 2b, the average building height (of only the buildings) is 49.8m. However, the metric used in this project will be an average calculated across the entire area of the domain producing, in this case, an average building height of 30.0m.

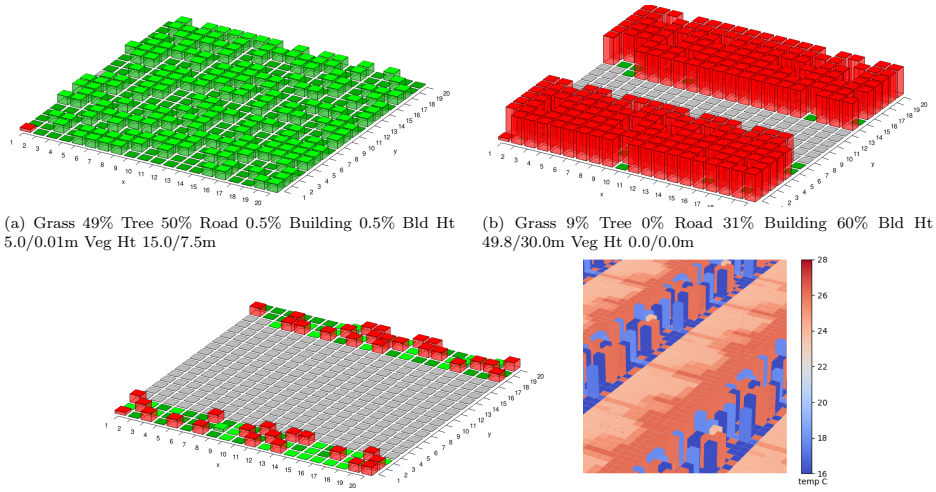

(a) Grass 49% Tree 50% Road 0.5% Building 0.5% Bld Ht 5.0/0.01m Veg Ht 15.0/7.5m

(b) Grass 9% Tree 0% Road 31% Building 60% Bld Ht 49.8/30.0m Veg Ht 0.0/0.0m

(c) Grass 9% Tree 10% Road 71% Building 10% Bld Ht 14.8/1.5m Veg Ht 0.5/0.05m

(d) UTCI at 2pm Feb 12, 2004

Figure 2: **Three example scenarios (panels a, b, and c) from the 9814 modelled in the project. Building heights are given as average heights of buildings and a height averaged across the domain. Vegetation heights follow the same pattern. d) Modelled 3-dimensional results of UTCI for scenario (c) at 2pm February 12, 2004. Note, VTUF-3D nests a central area of interest in 9 identical surrounding areas and this visualisation includes some of these nested results (and at a different rotation than the scenarios).**

2.2. VTUF-3D

VTUF-3D (Nice et al., 2018) was used as the micro-climate modelling tool for this study. VTUF-3D is a urban micro-climate surface energy balance model that incorporates vegetation physiological processes and shading effects. The model provides output of a canyon averaged air temperature (T_{can}) as well as spatial 3-dimensional values for surface temperature (T_{surf}), mean radiant temperature (T_{mrt}), and the universal thermal climate index ($UTCI$) (Figure 2d). Scenarios were run with a 5m resolution and were forced by observations from Preston in Melbourne from Coutts et al. (2007) over the five days February 9-13, 2004. The VTUF-3D model has undergone a comprehensive validation process (Nice, 2016; Nice et al., 2018) using this forcing data.

February 12, 2004 was chosen as a comparison day for the analysis. The forcing data for this day is presented in Figure 3. Air temperatures on this day reached 26°C, which is close to the climatological mean maximum temperature for Melbourne (25.8°C). February 12th was chosen as a representative warm summer day with clear sky conditions across the entire day. The combination of air temperature and incoming shortwave radiation caused some periods of heat stress. Many heat mitigation assessments concentrate on extreme heat days, however, in cities like Melbourne, even days close to the climatological mean can cause levels of heat stress, especially within some urban morphologies (i.e. large amounts of unshaded impervious surfaces). Further, the number of days similar to February 12th, where some level of heat stress and thermal discomfort can be experienced, far exceed the number of extreme heat days. For example, in Melbourne over 2015-2020, the average number of days per year that exceed 35°C are 11 compared to 80 days per year that exceed 25°C (Bureau of Meteorology, 2021).

2.3. Comprehensive urban form analysis

To determine the influence of each parameter on heat stress and urban thermal conditions, a sensitivity analysis was performed on the full range of parameters (fractions of grass, street, building, and vegetation as well as average vegetation and building heights). VTUF-3D generates a single canyon averaged air temperature (T_{can}), therefore a single (well mixed) air temperature value was extracted for each timestep from the 9814 completed model runs. Additional temperature results are spatially distributed in 3-dimensions across all the surfaces in the scenario. A slice at 0m (ground level) was extracted for $UTCI$ and a domain mean value calculated for each timestep for each scenario. Full 3-dimensional results were also extracted for later use in Sections 2.3.1 and 2.4.

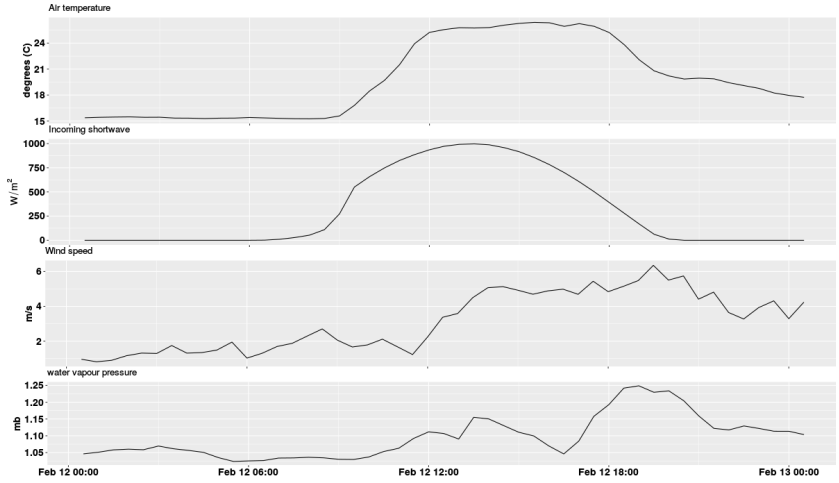

Figure 3: **Forcing data (air temperature, incoming shortwave, wind speed, and water vapour pressure) for February 12, 2004, the day of interest used in the analysis.**

2.3.1. Temperature trends and feature importance due to surface fractions and average heights

To determine the temperature trends (T_{can} and $UTCI$) across all the scenarios, box plots were generated (using Matplotlib (Hunter, 2007)) of modelled temperature results vs. surface types (tree, grass, building, road) grouped by 10% ranges as well as average building and vegetation heights (grouped by 0.4m ranges). Rankings of feature importance (the influence each features has on predicting a target variable) were determined (using Random Forest Classifier from scikit-learn (Pedregosa et al., 2011)) for each temperature type (T_{can} and $UTCI$) for the four surface fraction parameters (grass, trees, buildings, and roads) and average vegetation and building heights at each hour during the simulations. The backgrounds of each plot were tinted darker green where a parameter scored higher in feature importance.

Plots were generated for each 1 hour timestep using the extracted T_{can} result from the 9814 scenarios and the calculated $UTCI$ domain mean at 0m for all the scenarios. February 12, 2004 5am and 2pm were chosen as representative timesteps for nighttime and daytime and are presented in Section 3.1. To explore the trends associated with each surface fraction type across a diurnal cycle, the representative day of February 12, 2004, mean temperatures were calculated for T_{can} and $UTCI$ and fraction percentages and heights (using the pandas (pandas development team, 2020) describe method and groupby) in 10% increments of surface fractions or 0.8 meter average heights. Then temperature differences between increasing fractions and heights were calculated and plotted across the entire diurnal cycle of 12 February 2004. This allows the relationship between a surface type, its fractional amount, the time of day, and the temperature outcome to be seen and are presented in Section 3.1.

2.4. Distributions of temperatures across a diurnal cycle

As an illustration of the variability of UTCI temperatures across scenarios and hourly across the diurnal cycle of February 12th, the distributions of some selected scenarios are plotted (using ggridges (Wilke, 2020)) and presented in Section 3.2. These scenarios represented a range of urban morphologies found in Melbourne.

2.5. City scale heat maps from micro-climate modelled results

To show the applied usage of the systematic modelling, city-wide heat maps of T_{can}, T_{sfc}, and $UTCI$ were generated from the 9814 modelled scenario results. Each model run was forced by the observations of Preston in Melbourne from Coutts et al. (2007) over the days February 9-14, 2004. Geoscape (Geoscape, 2020), from the Public Sector Mapping Agency (PSMA) Australia, provides 2 meter resolution land cover (road, building, grass, bare earth, etc) as well as building and tree footprints and heights were used. From this, surface fractions and average building and vegetation heights were calculated for 100×100m locations across Melbourne, Sydney, Adelaide, Brisbane, and Perth. The actual urban morphology parameters calculated from the Geoscape data were matched to the modelled scenario with the

closest matching parameters of surface fractions and average heights for each 100×100m location and visualized (using R package sf (Pebesma, 2018)). Locations with greater than 10% surface fraction of water were removed from the results as VTUF-3D does not currently model water bodies. These resulting heatmaps (only Melbourne and Sydney are presented) show a city-wide assessment of thermal performance due to urban form but are independent of local weather conditions (i.e. ocean breezes vs. calm inland conditions) and topography (differing elevations across the cities). T_{sfc} heatmap results were also compared to the land surface temperature (LST) maps of Melbourne and Sydney from Landsat 8. All Landsat 8 imagery corresponds to 10am local time. Images were selected for cloudless days that most closely matched forcing conditions. Melbourne images were from December 11, 2018 (air temperatures minimum and maximums of 22 and 26°C). Sydney images were from March 11, 2019 (air temperatures minimum and maximums of 22 and 26°C).

3. Results

3.1. Temperature trends across fractions and feature importance

In Figure 4, T_{can} temperatures for all scenarios are shown for ranges of fractions and heights across the diurnal cycle of 14 February 2004. These have been clustered into 10% surface fraction ranges or 0.8m height ranges (i.e. 20% includes the range 10 to 20% while 1.6m includes 0.8 to 1.6m). Small differences (1°C) are seen at night-time, with larger ranges seen with street fractions and to a lesser degree with building fractions and building heights (temperature reductions with grass, increases with all other types). After dawn, the differences begin to increase and reaching a peak at mid-day with maximum differences of approximately 5°C with grass, tree, building fractions and building and vegetation heights. Differences at mid-day reach maximum divergences of 10 and 15°C as street surface fractions reach 80 and 90% respectively. Building and street fractions and building heights drive temperature increases while other types drive reductions.

For surface fraction and height clusters across 14 February 2004 of $UTCI$ (Figure 5), which includes the influence of surface temperature (T_{sfc}) and mean radiant temperature (T_{mrt}), the night-time ranges show wider differences. Increasing building heights, building fractions, and street fractions drive temperature increases both day and night while other types drive reductions. All fractions and heights show a difference of 3°C and greater between the lowest and highest amounts of fractions and heights. These difference remain roughly similar through dawn and until about 8am. Street fractions are the exception and show even wider divergences (5°C and more) starting at 6am. After 6am, differences widen to 5°C for building fractions and building heights and 10°C for tree and grass fractions and vegetation heights. Meanwhile, differences for street fractions grow to nearly 15°C for 80% and over 20°C for 90%.

The range of average results from all scenarios for two temperature types (T_{can} and $UTCI$) at varying surface fractions of grass, trees, buildings, and roads and average heights of vegetation and buildings are shown in Figures 6(a,c), 6(b,d) on February 12, 2004 at 5am and 2pm respectively. Note, the number of possible surface type combinations decreases as a single surface type approaches 100%. For example, 90% grass leaves only a small number of combinations for the remaining 10% surface cover. Although, for each of these surface fraction combinations, there are a range of scenarios with varying vegetation and building heights.

During the nighttime (represented by 5am), there is a narrow range of T_{can}, from approximately 15.3-16.3°C. Increasing fractions of trees has a slight warming impact with an increase of approximately 0.2°C when increasing trees from 0 to 100%. Increasing vegetation height has a similar impact at nighttime. Increasing building heights has an almost identical effect. Increasing building and street fractions has a mostly neutral effect but at dawn (5am), the increasing street fractions start to have a very slight warming impact (0.3°C). Increasing grass fractions has a slight cooling impact of about 0.3°C.

At 2pm, at the warmest time of the day, increasing tree and building fractions and increasing vegetation height continue to provide T_{can} temperature reductions of 1-2°C. Grass fractions and building heights increases show an initial reduction towards the middle fraction ranges then an increase at the higher ranges, with a reduction in the middle ranges of approximately 1°C. Increases in street fractions however show a rapid increase in T_{can} temperatures of approximately 3°C as street fractions approach 80% and another 3°C at 90%.

At 2pm, trends of $UTCI$ amplify the trends seen with T_{can}. Increases in street fractions show increases of approximately 6°C as street fractions approach 80% and another 6°C at 90%. Increasing grass and building heights shows increases of 5°C as fractions or heights increase. Increasing tree and building fractions and tree heights show reductions in temperatures of approximately 5°C.

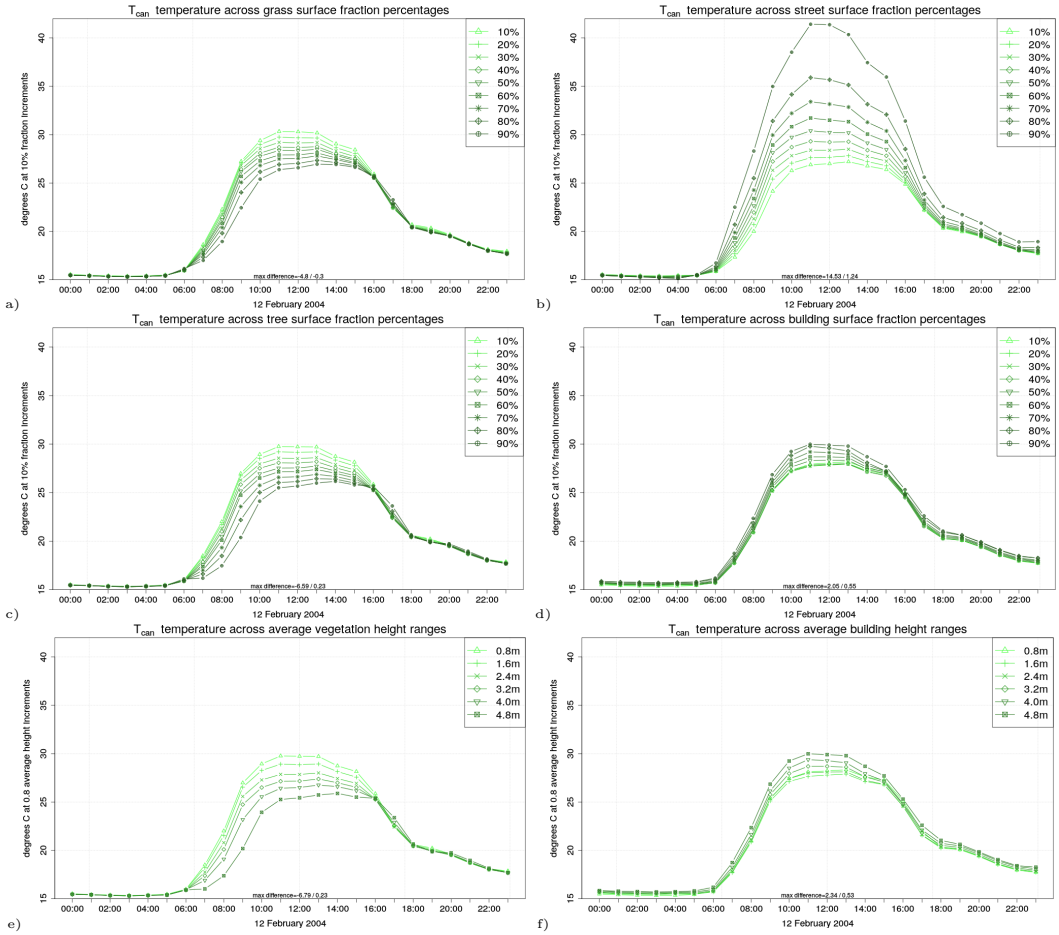

Figure 4: **Mean T_{can} outcomes clustered by 10% surface fraction ranges of a) grass, b) streets, c) trees, and d) buildings and e) average vegetation and f) average building heights clustered by 0.8m increases over a diurnal cycle of February 12, 2004. The clusters contain fractions up to the fractional or height breakpoint (i.e. 20% includes the range 10 to 20% while 1.6m includes 0.8 to 1.6m). Annotated maximum difference values for each panel shows the maximum difference between 90% and 10% fractions or 4.8m and 0.8m heights for daytime(6am-10pm)/nighttime (10pm-6am).**

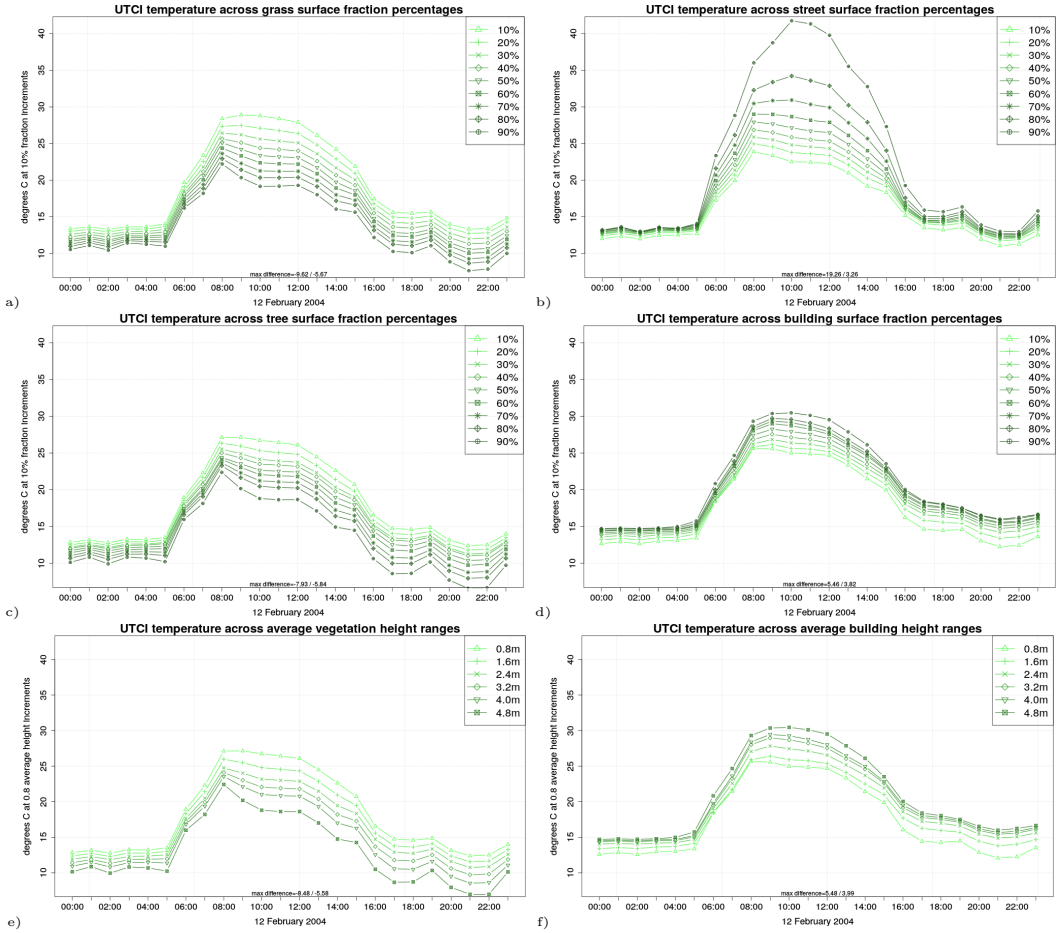

Figure 5: **Mean *UTCI* outcomes clustered by 10% surface fraction ranges of a) grass, b) streets, c) trees, and d) buildings and e) average vegetation and f) average building heights clustered by 0.8m increases over a diurnal cycle of February 12, 2004. The clusters contain fractions up to the fractional or height breakpoint (i.e. 20% includes the range 10 to 20% while 1.6m includes 0.8 to 1.6m). Annotated maximum difference values for each panel shows the maximum difference between 90% and 10% fractions or 4.8m and 0.8m heights for daytime(6am-10pm)/nighttime (10pm-6am).**

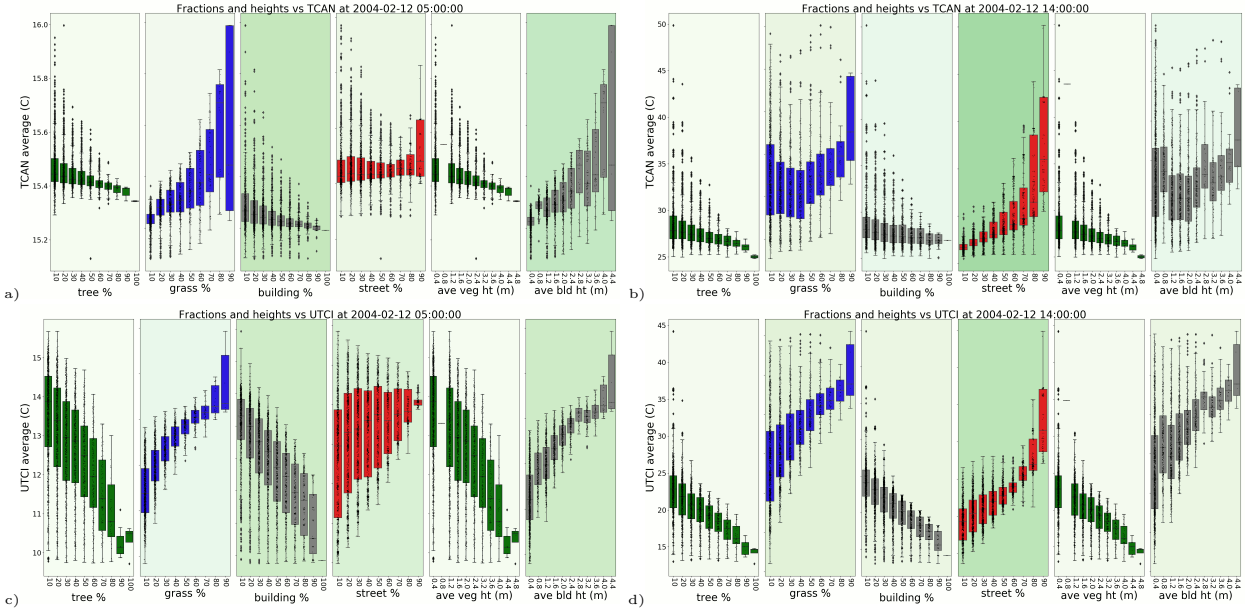

Figure 6: **Surface fractions percentages (trees, grass, buildings, and streets) and average heights (vegetation and building) vs. T_{can} (top) and $UTCI$ (bottom) for February 12, 2004, 5am (left) and 2pm (right). The clusters will contain fractions up to the fractional or height breakpoint (i.e. 20% includes the range 10 to 20% while 1.6m includes 1.2 to 1.6m). Feature importance for each temperature type is indicated by the green background tinting.**

Temperature	Time	↑ Trees	↑ Grass	↑ Bld	↑ Street	↑ Veg Ht	↑ Bld Ht
T_{can}	Night	**0.2**	-0.3	**0.6**	**1.2**	**0.2**	**0.5**
T_{can}	Day	-6.6	-4.8	**2.1**	**14.5**	-6.8	**2.3**
$UTCI$	Night	-5.8	-5.7	**3.8**	**3.3**	-5.6	**4.0**
$UTCI$	Day	-7.9	-9.6	**5.5**	**19.3**	-8.5	**5.5**

Table 1: Maximum differences (°C) in T_{can} and $UTCI$ when increasing fractions from 10% to 90% and average vegetation and building heights to 4.4m. Bold indicates temperatures increase as fractions or heights increase. From maximum difference annotations in Figures 4 and 5

At nighttime, trends of $UTCI$, which include the influences of T_{sfc} and T_{mrt}, show decreases of approximately 2.5°C as fractions of trees and buildings and vegetation heights increase. $UTCI$ increases approximately 3.0°C as grass fractions and building heights increase and 1.5°C as street fractions increase.

Highlighted results are summarised in Table 1, taken from maximum difference annotations in Figures 4 and 5. Analysis of feature importance shows that building fractions and building heights are most significant for T_{can} (Figure 7a) at night while building fractions and building heights are slightly more important than grass and streets and trees and vegetation heights are of the lowest importance for $UTCI$ (Figure 7b). During the daytime, street fractions are of the highest importance for both T_{can} and $UTCI$.

3.2. Distributions of temperatures across a diurnal cycle

Figure 8 shows the $UTCI$ distributions for a number of selected scenarios across the 24 hours of February 12, 2004. The preceding results (Section 3.1) are based on mean values, averaged across the ground level results across each domain. However, different mixes of surface fractions and average heights result in widely varying distributions of temperatures (all in °C).

Figure 8a presents a scenario with very low fractions of roads and buildings and as a result shows $UTCI$ temperatures mostly clustered in the lower ranges across day and night and very few locations that exceed the mid 20s during the day. Figure 8b shows a scenario with a moderate amount of streets and buildings (20% and 30%) and moderate building heights, but yields similar results to Figure 8a. Figure 8d, with higher amounts of buildings and roads, shows

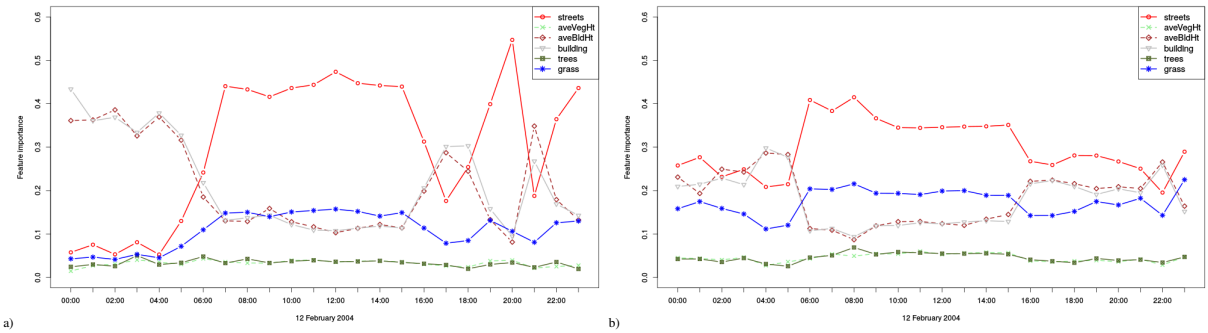

Figure 7: **Feature importance in a)** T_{can} **and b)** $UTCI$ **for the four surface fractions of streets, buildings, trees, and grass and average heights of vegetation and buildings across February 12, 2004.**

a strong shift towards predominately hotter $UTCI$ temperatures (30°C) across the entire domain during the daytime (also reflected in the median), while Figure 8c, with slightly higher fractions of vegetation, shows a similar distribution but the median is much lower (in the lower 20s°C).

These four example distributions show that urban heat has high variability at a micro-scale, even between scenarios with similar urban form and surface fractions. Mean temperature values (such as Table 1) can show general trends but each of these four distributions will contribute to four very different spatial experiences of urban heat and human thermal stress in each area.

4. Discussion

4.1. The influence of urban surfaces on urban heat

Studies providing a systematic examination of the influence of varying surface fractions and urban heights are rare and generally based on remote sensing data. In this study, through systematic micro-climate modelling of a comprehensive range of surface fractions and average heights, the importance and relative influence of each feature type on the temperature types of T_{can} and $UTCI$ was examined. For T_{can}, at night time, a narrow range of temperature variations were found, of approximately 1.0°C. Increasing fractions of trees had a limited impact at midnight and contributed to a very slight increase (+0.2°C) at dawn. Increasing building heights had a warming impact (+1.2°C) while grass drove a slight cooling (-0.3°C). Increasing street fractions contributed to a warming effect (+0.3°C) at dawn. Building fractions and building heights were found to be the most significant features at night time. During the daytime, the most important feature was the fraction of streets. Street fractions of 80 and 90% can drive T_{can} increases of up to 10 and 15°C respectively while reductions are seen of about -5°C when increasing grass and tree fractions from 0 to 100%.

While other studies show similar findings, often they were only able to demonstrate temperature trends rather than more detailed relationships. Emery et al. (2021), in their observations of the influence of different LCZ classes on air temperature, found that the LCZ classes with the warmest air temperatures were those dominated by artificial, mineral, and impervious surfaces, while LCZ classes with vegetation were the coolest. However, they were not able to quantify the ranges of temperatures in more detail resulting from the different classes. Using remotely sensed LST, Alexander (2021) classified areas in a number of Danish cities into two classes of buildings and vegetation (essentially impervious vs. pervious) and into ranges of vegetation and building heights and examined their influence on LST. He found LST reduced by approximately 4°C when vegetation fractions increased from 0-5 to 95-100% and increased by 4°C when building fractions increased by the same. Also, vegetation height had negative correlation with LST but vegetation cover was found to be a stronger predictor. Building height had a positive correlation with LST, but only up to 9m, and was not always found to have a strong influence on LST in some of the studied cities.

Peng et al. (2022) found, using a Random Forest regression of MODIS LST observations of a highly urbanised city in Japan, the feature importance to predict urban heat island intensity in the daytime was highest for building density followed by distance to green space while at night time distance to green space was the most important followed by distance to water and road density. In another study, using Landsat derived LST of different LCZ classes across

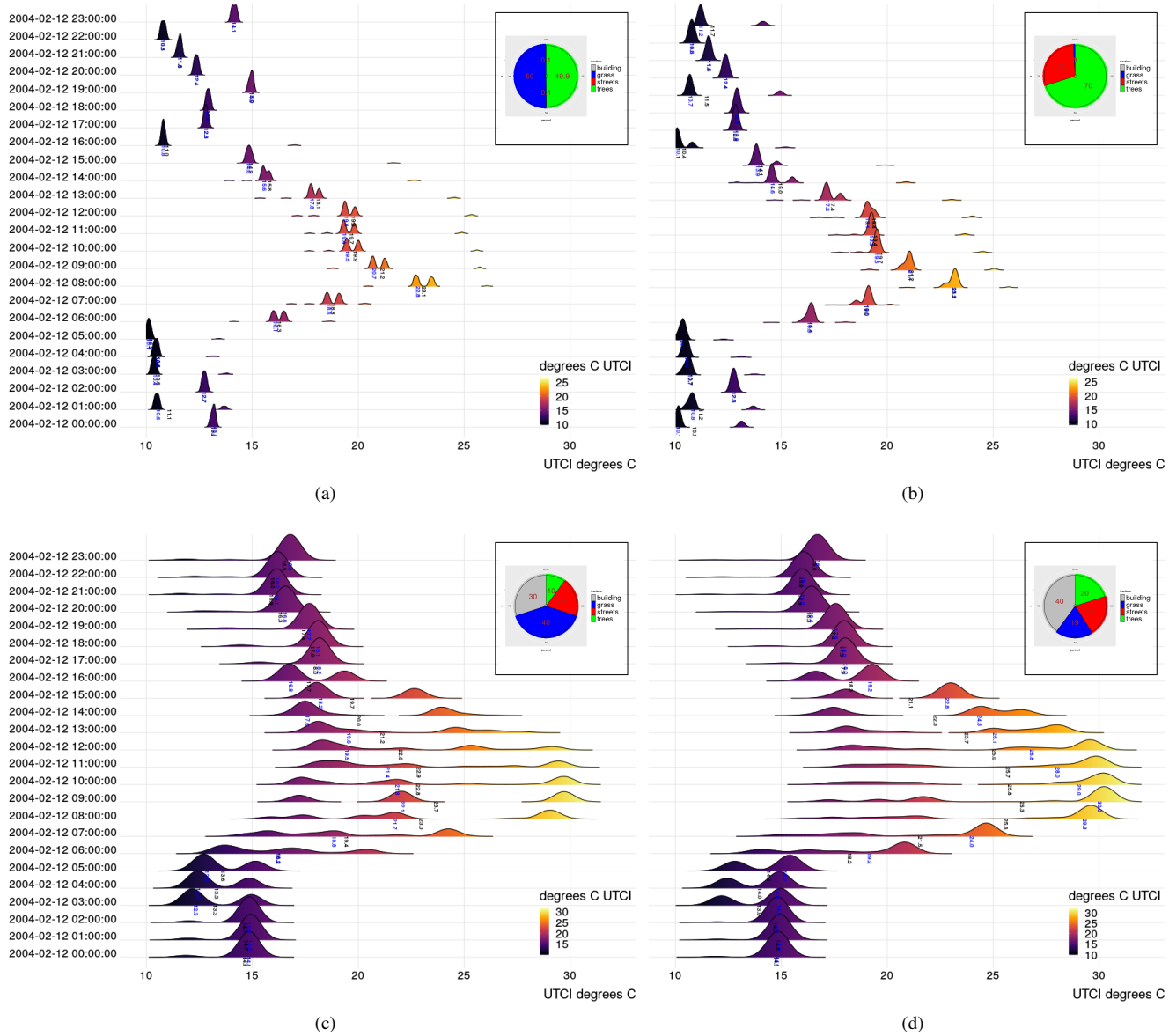

Figure 8: **Distribution of $UTCI$ across February 12, 2004 for scenarios a) 50% grass, 49.99% trees, 0.01% road, 0% building, average vegetation height of 4m, and average building height of 0m, b) 29% grass, 69% trees, 1% road, 1% building, average vegetation height of 0.5m, and average building height of 5m, c) 40% grass, 10% trees, 20% road, 30% building, average vegetation height of 2m, and average building height of 14m, and d) 19% grass, 20% trees, 21% road, 40% building, average vegetation height of 1m, and average building height of 9m. Insert shows percent fractions of surface types. Hourly medians are annotated in blue and hourly means in black.**

four African cities (Li et al., 2022), the highest LST temperatures were found in the urban typologies of compact mid-rise, compact low-rise, and large low-rise (LCZ2, 3, and 8) and lowest in dense trees and water (LCZA and G). They found statistically significant differences between the LCZs, but not always when comparing LCZ classes in different cities of different Köppen climate classifications, where often compact midrise (LCZ2) and open midrise (LCZ5) typologies were coolest (due to higher building heights). The LCZ typologies were found to be useful across single cities but could not always reliably be used to compare LCZ classes across different cities, especially those with differing climates.

While these results are able to show broad trends due to differing amounts of surface fractions, they cannot entirely predict the influences on thermal comfort at the ground level, underneath the urban canopy where surface temperatures are moderated by shading from vegetation and buildings. This is a limitation of remotely sensed LST observations, that can only provide the temperatures at the top of the urban canopy. Some studies are able to provide some additional data on the under canopy impacts through observations. For example, micro-climate observations from Broadbent et al. (2017) showed that in a residential suburb, T_{sfc} temperatures of concrete, buildings, and bare ground were 2.4, 3.1, and 1.1°C hotter than the area averages during the day and areas with trees, irrigated grass, and low vegetation were 3.0, 7.7, and 6.8°C cooler. While high resolution spatial air temperature are difficult to observe, Broadbent et al. (2017) also found increases over the suburb average in air temperature of 1°C in the cluster type of urban mid-rise and 0.5°C with the type urban residential. They also found an irrigated grass daytime cooling effect of -0.1°C per 5% fraction increase. Middel and Krayenhoff (2019) found trees could provide large reductions in T_{mrt} on extreme heat days, with reductions up to 33.4°C and with sky view factor (SVF) highly influential in determining the reductions, 4°C T_{mrt} reductions per 0.1 SVF decreases. However, the trade-offs are a warming effect at night of up to 5°C. In addition, they found replacing impervious with pervious surfaces can decrease T_{mrt} by 1.0-1.5°C per tenth of land converted and unshaded irrigated grass could reduce T_{mrt} by more than 10°C compared to impervious surfaces with unirrigated grass providing still about half as much in reductions. Additionally, Krayenhoff et al. (2021) finds that trees provide additional 0.3°C reductions per 0.10 canopy cover increase.

4.2. City scale heat maps from micro-climate modelled results

Following on from the results of the comprehensive urban form analysis and reflecting many of the specific findings of other studies of the impact of differing types of urban form on urban heat, the modelled results underlying this analysis were applied to demonstrate their application to a city-wide heat mapping exercise. These heat maps show the impact of present day urban form across a number of Australian cities, isolated from geography, topography, and local weather conditions. Figure 9 shows city-wide heat maps of T_{can} and $UTCI$ in Melbourne at 2pm on February 12, 2004 constructed by matching the closest matching parameters for each locations from the 9814 modelled scenario results. A narrow range of air temperatures are seen across most of the city, closely aligned to the modelling forcing temperature at 2pm of 25.9°C. Higher temperatures can be seen in areas corresponding to higher fractions of roads and to a lesser degree of buildings. No particular reductions of air temperatures are seen in areas corresponding to higher levels of trees or grass surface fractions. Fractional breakdowns of surfaces types across Melbourne are shown in Supplementary Figure S1.

Wider ranges of surface temperatures are seen across Melbourne. Some slight reductions of surface temperatures (below the forcing air temperature) are seen in areas that correspond to higher fractions of grass and of trees. However, strong increases in surface temperatures in areas with higher fractions of street surfaces, even in areas with street fractions as low as 30%. Very strong increases in surface temperatures can be seen in areas with high street surface fractions, for example Melbourne Airport in the north west, the central business district (CBD) in the city centre, and Moorabbin Airport in the city south east.

Figure 10 presents a comparison of modelled T_{sfc} to Landsat 8 LST data. Figure 10a shows Landsat 8 imagery captured on a cloudless day that mostly closely corresponds to the modelled conditions, 10am December 11, 2018 when local conditions of air temperature on this day were minimum and maximum of 22 and 26°C. Figure 10b shows T_{sfc} created from modelled results at 10am on February 12, 2004 and February 14, 2004.

In comparing the constructed T_{sfc} heat maps with the LST imagery, some observations can be made. However note, the two datasets measure different things and might not be entirely comparable. LST observations are captured by satellite and correspond to temperatures at the top of the urban canopy (i.e. the tops of trees and buildings) while the modelled T_{sfc} corresponds to ground surface temperatures and will generally be cooler as they include areas that are shaded by tree canopies and buildings. In addition, LST observations are influenced by additional factors than

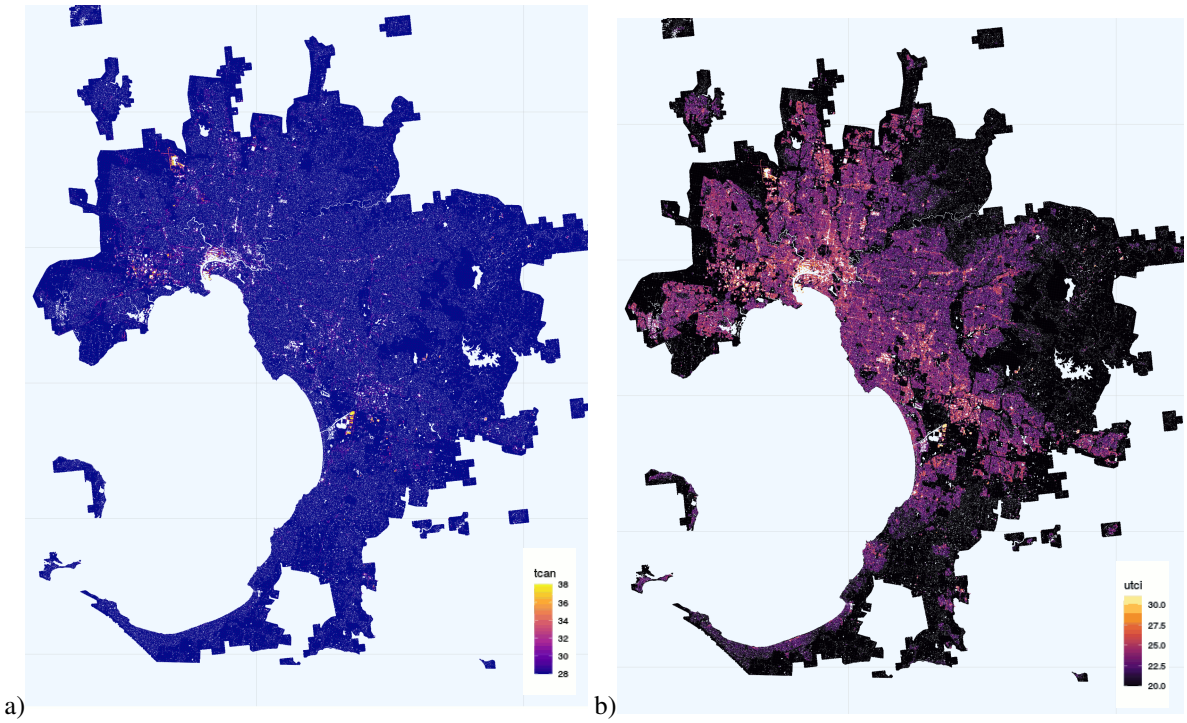

a) b)

Figure 9: **a)** T_{can} **and b)** $UTCI$ **heatmaps on February 12, 2004 at 2pm generated by matching the closest matching parameters of surface fractions and average heights for each 100×100m location in Melbourne from 9814 modelled scenario results (in** °C**).**

just the urban form including topography and localised weather conditions. In Figure 10a, the cooler locations in the LST observations mostly include locations immediately off the coast and in the eastern fringes of Melbourne, the Dandenong Ranges which range from 500m to over 1000m in elevation, while the majority of central and inner Melbourne is under 100m in elevation. The main differences between the LST observations and the modelled results are strongly related to the surface fraction types, which a strong correlation between the differences and building and street fractions and a strong negative correlation with grass surface fractions.

Additionally, heat maps were generated for other cities. Using the 9814 modelled scenario results, heat maps of T_{can} and $UTCI$ (Supplementary Figure S3) were created for Sydney for February 12, 2004 at 2pm by matching the closest matching parameters, as calculated from Supplementary Figure S2, for each location. Supplementary Figure S4a shows cloudless Landsat 8 observations from 10am March 11, 2019 (local conditions of air temperature on this day were minimum and maximum of 22 and 26°C) while Supplementary Figure S3b shows T_{sfc} heatmaps created from modelled results at 10am on February 12, 2004.

The results are similar to those from Melbourne. Ranges of T_{can} are generally very narrow with small localised hot spots. The LST observations reflect a different topography than Melbourne with a larger influence of coastal features and a smaller range of elevations. Much of the central city is under 100m and only approaching 200m in the north east areas. The areas with higher ranges of LST are concentrated in the agricultural western regions of the city (with very high percentages of grass/low vegetation land cover fractions). Similar to Melbourne, correlations between differences between LST and T_{sfc} are strongly negatively correlated with grass fractions but somewhat less correlated with building and street fractions.

5. Conclusion

Observational studies have previously attempted to quantify the influence of urban form on urban heat largely using two different types of observations, top of the urban canopy remotely sensed LST and under the urban canopy ground level micro-scaled observations. Micro-scaled ground based observations can provide detailed assessments

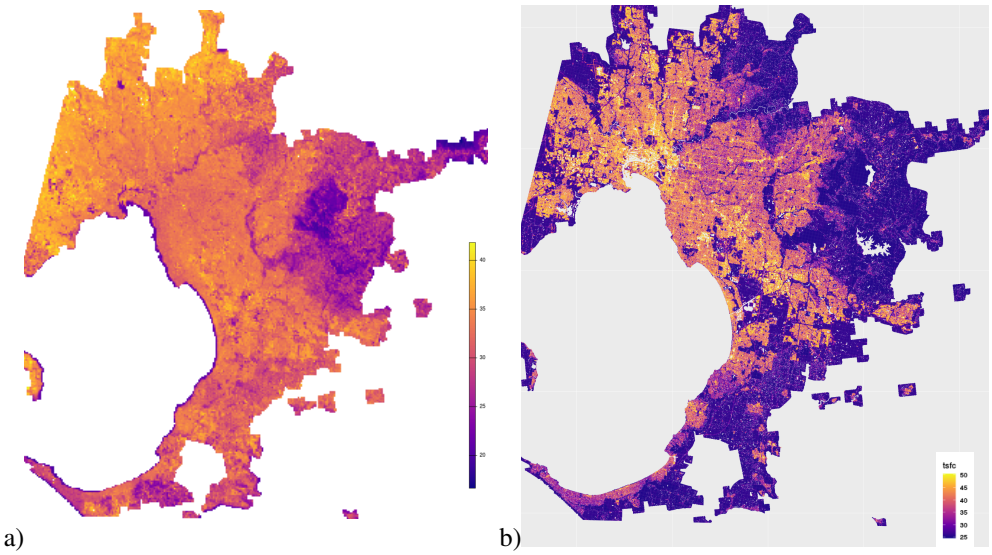

Figure 10: **a) Landsat 8 land surface temperature (°C) captured 10am December 11, 2018. Local conditions of air temperature on this day were minimum and maximum of 22 and 26°C. b) Modelled T_{sfc} (°C) on February 12, 2004 at 10am generated by matching the closest matching parameters of surface fractions and average heights for each 100×100m location in Melbourne from 9814 modelled scenario results.**

under the canopy, but are time-intensive, requiring substantial effort to collect, and are difficult to scale up to a city-wide scale. The observations from other studies demonstrate the usefulness of the results and the application of the systematic modelling in this study. The observations show many of the trends found in this study, including the large increases in both T_{can} and $UTCI$ with increasing road fractions, as well as decreases of both temperature types during the daytime with increasing vegetation fractions and heights. Our method also overcomes difficulties encountered with the LCZ-based observations and modelling assessments, where the highly urbanised classes were found to be hotter while the natural classes were cooler, findings in line with our results. However, due to the broad ranges each LCZ can represent along with the (often non-linear) interactions between the parameters, detailed and specific quantifications have not always been possible in the studies utilising LCZs (i.e. Emery et al. (2021)). Our method allows the influence of elements of urban form to be quantified as heights and fractional amounts of land cover are incrementally increased and decreased.

Using the comprehensive urban form analysis methods in this study allows a determination of the importance and relative influence of each surface type and feature height on thermal performance (e.g. increasing street fractions from 50% to 80% can drive air temperature increases of up to 5°C). Additionally, once these relationships have been quantified, it becomes possible to apply the results across a broad area, a city-wide assessment of thermal comfort. This is an area of broad interest as evidenced by the numerous studies attempting this through satellite observed LST. But the modelled approach eliminates the difficulty using top of the canopy LST observations to derive ground level temperatures, temperatures that also include the shading impacts of the urban canopy. More importantly, it removes geographic influences (such as topography, ocean effects, and local weather) from the results and allows an assessment based solely on the urban and natural forms of the urban areas. This allows mitigation strategies to be tested based on the urban form elements that can be changed, while removed from influences that cannot be redesigned. In addition, the ability to capture at high temporal and spatial scales the high variability of elements of urban heat (i.e. the distributions of $UTCI$ in different scenarios in Figure 8) point to new directions for future research. Urban areas can be characterised by the quality of their connectedness of cooling and how well each area supports pedestrians navigating urban arrangements to minimise their thermal stress.

In addition, future work can address one potential limitation of this study. VTUF-3D has been extensively evaluated using the forcing data used in this study, but like all models, has biases. Is is possible that VTUF-3D is underestimating temperatures of grass. The correlations between the surface fractions and differences between observed LST and modelled T_{sfc} suggest that the temperature trends for streets (0.69 and 0.72 in Melbourne) and buildings (0.78

and 0.72 in Melbourne) are reasonable but the magnitude is too high while grass (-0.80 and -0.85) trends are also reasonable but too low. Meanwhile the correlations for trees are very low suggesting the variations are not regular. As the percent fractions for trees just suggests that tree cover exists, it does not fully characterise the tree cover, such as the level of canopy cover (i.e. a leaf area index). VTUF-3D is undergoing continuous improvement, especially its vegetation scheme. The overall method in this study can be repeated using this or other improved micro-climate models in future work.

6. References

Alexander, C., 2021. Influence of the proportion, height and proximity of vegetation and buildings on urban land surface temperature. International Journal of Applied Earth Observations and Geoinformation 95, 102265.
URL https://doi.org/10.1016/j.jag.2020.102265

Aniello, C., Morgan, K., Busbey, A., Newland, L., 1995. MAPPING MICRO-URBAN HEAT ISLANDS USING LANDSAT TM AND A GIS. Computers & Geosciences 21 (8), 965–969.

Bowler, D. E., Buyung-Ali, L., Knight, T. M., Pullin, A. S., 2010. Urban greening to cool towns and cities: A systematic review of the empirical evidence. Landscape and Urban Planning 97 (3), 147–155.

Broadbent, A. M., Coutts, A. M., Tapper, N. J., Demuzere, M., Beringer, J., 2017. The microscale cooling effects of water sensitive urban design and irrigation in a suburban environment. Theor. Appl. Climatol., 1–23.

Bröde, P., Fiala, D., Blazejczyk, K., Holmér, I., Jendritzky, G., Kampmann, B., Tinz, B., Havenith, G., 2012. Deriving the operational procedure for the Universal Thermal Climate Index (UTCI). International Journal of Biometeorology 56 (3), 481–494.

Bruse, M., 1999. The influences of local environmental design on microclimate- development of a prognostic numerical Model ENVI-met for the simulation of Wind, temperature and humidity distribution in urban structures. Ph.D. thesis, University of Bochum, Germany (in German).

Bureau of Meteorology, 2021. Long-term temperature record: Australian Climate Observations Reference Network - Surface Air Temperature (ACORN-SAT).
URL http://www.bom.gov.au/climate/data/acorn-sat/

Cheung, P. K., Livesley, S. J., Nice, K. A., 2021. Estimating the cooling potential of irrigating green spaces in 100 global cities with arid, temperate or continental climates. Sustainable Cities and Society, 102974.
URL https://doi.org/10.1016/j.scs.2021.102974

Ching, J., Aliaga, D., Mills, G., et al., 2019. Pathway using WUDAPT's Digital Synthetic City tool towards generating urban canopy parameters for multi-scale urban atmospheric modeling. Urban Climate 28, 100459.
URL https://www.sciencedirect.com/science/article/abs/pii/S2212095519300975

Ching, J., Mills, G., Bechtel, B., See, L., Feddema, J., Wang, X., Ren, C., Brousse, O., Martilli, A., Neophytou, M., Mouzourides, P., Stewart, I., Hanna, A., Ng, E., Foley, M., Alexander, P., Aliaga, D., Niyogi, D., Shreevastava, A., Bhalachandran, P., Masson, V., Hidalgo, J., Fung, J., Andrade, M., Baklanov, A., Dai, W., Milcinski, G., Demuzere, M., Brunsell, N., Pesaresi, M., Miao, S., Mu, Q., Chen, F., Theeuwes, N., 2018. World Urban Database and Access Portal Tools (WUDAPT), an urban weather, climate and environmental modeling infrastructure for the Anthropocene. Bulletin of the American Meteorological Society, BAMS–D–16–0236.1.
URL http://journals.ametsoc.org/doi/10.1175/BAMS-D-16-0236.1

Coates, L., Haynes, K., O'Brien, J., et al., 2014. Exploring 167 years of vulnerability: An examination of extreme heat events in Australia 1844-2010. Environmental Science and Policy 42, 33–44.
URL http://dx.doi.org/10.1016/j.envsci.2014.05.003 https://www.sciencedirect.com/science/article/pii/S1462901114000999

Coffel, E. D., Horton, R. M., de Sherbinin, A., 2018. Temperature and humidity based projections of a rapid rise in global heat stress exposure during the 21st century. Environ. Res. Lett. 13, 014001.

Coutts, A. M., Beringer, J., Tapper, N. J., 2007. Impact of Increasing Urban Density on Local Climate: Spatial and Temporal Variations in the Surface Energy Balance in Melbourne, Australia. Journal of Applied Meteorology and Climatology 46 (4), 477–493.
URL http://journals.ametsoc.org/doi/abs/10.1175/JAM2462.1

Coutts, A. M., Harris, R. J., Phan, T., Livesley, S. J., Williams, N. S., Tapper, N. J., 2016. Thermal infrared remote sensing of urban heat: Hotspots, vegetation, and an assessment of techniques for use in urban planning. Remote Sensing of Environment 186, 637–651.
URL http://dx.doi.org/10.1016/j.rse.2016.09.007

Coutts, A. M., Tapper, N. J., Beringer, J., Loughnan, M., Demuzere, M., 2012. Watering our Cities: The capacity for Water Sensitive Urban Design to support urban cooling and improve human thermal comfort in the Australian context. Progress in Physical Geography 37 (1), 2–28.
URL http://ppg.sagepub.com/cgi/doi/10.1177/0309133312461032

Coutts, A. M., White, E. C., Tapper, N. J., Beringer, J., Livesley, S. J., 2015. Temperature and human thermal comfort effects of street trees across three contrasting street canyon environments. Theoretical and Applied Climatology 124 (1), 55–68.
URL http://link.springer.com/10.1007/s00704-015-1409-y

Demuzere, M., Bechtel, B., Middel, A., Mills, G., 2019. Mapping Europe into local climate zones. PLoS ONE 14 (4), e0214474.
URL https://journals.plos.org/plosone/article?id=10.1371/journal.pone.0214474

Dominik, F., Andreas, M., 2019. Calculating human thermal comfort and thermal stress in the PALM model system 6.0. Geoscientific Model Development Discussions, 1–21.
URL https://www.geosci-model-dev-discuss.net/gmd-2019-202/

Duncan, J. M. A., Boruff, B., Saunders, A., Sun, Q., Hurley, J., Amati, M., 2018. Turning down the heat: An enhanced understanding of the relationship between urban vegetation and surface temperature at the city scale. Science of the Total Environment.
URL https://doi.org/10.1016/j.scitotenv.2018.11.223 https://www.sciencedirect.com/science/article/pii/S0048969718345790

Emery, J., Pohl, B., Cretat, J., Richard, Y., Pergaud, J., Rega, M., Zito, S., Dudek, J., Vairet, T., Joly, D., Thevein, T., 2021. How local climate zones influence urban air temperature: Measurements by bicycle in Dijon, France. Urban Climate 40, 101017.

Erell, E., Williamson, T., 2006. Simulating air temperature in an urban street canyon in all weather conditions using measured data at a reference meteorological station. International Journal of Climatology 26 (12), 1671–1694.
URL http://onlinelibrary.wiley.com/doi/10.1002/joc.1328/abstract

Geoscape, 2020. Australian Spatial data for 3D buildings, building heights & land parcels. https://geoscape.com.au/.

Hammerberg, K., Brousse, O., Martilli, A., Mahdavi, A., 2018. Implications of employing detailed urban canopy parameters for mesoscale climate modelling: a comparison between WUDAPT and GIS databases over Vienna, Austria. International Journal of Climatology 38, e1241–e1257.

Hendel, M., Gutierrez, P., Colombert, M., Diab, Y., Royon, L., 2016. Measuring the effects of urban heat island mitigation techniques in the field: Application to the case of pavement-watering in Paris. Urban Climate 16, 43–58.
URL http://dx.doi.org/10.1016/j.uclim.2016.02.003

Hunter, J. D., 2007. Matplotlib: A 2D graphics environment. Computing In Science & Engineering 9 (3), 90–95.

IPCC, 2013. Climate Change 2013: The Physical Science Basis. Contribution of Working Group I to the Fifth Assessment Report of the Intergovernmental Panel on Climate Change. Tech. rep., Intergovernmental Panel on Climate Change, Cambridge, United Kingdom and New York, NY, USA.

Jacobs, S., Gallant, A., Tapper, N., Li, D., 2018. Use of cool roofs and vegetation to mitigate urban heat and improve human thermal stress in Melbourne, Australia. J. Appl. Meteor. Climatol.
URL https://journals.ametsoc.org/doi/abs/10.1175/JAMC-D-17-0243.1

Kántor, N., Unger, J., 2011. The most problematic variable in the course of human-biometeorological comfort assessment - the mean radiant temperature. Open Geosciences 3 (1), 90–100.

Krayenhoff, E. S., Broadbent, A. M., Zhao, L., Georgescu, M., Middel, A., Voogt, J. A., Martilli, A., Sailor, D. J., Erell, E., 2021. Cooling hot cities: A systematic and critical review of the numerical modelling literature. Environ. Res. Lett.

Lee, I., Voogt, J., Gillespie, T., 2018. Analysis and Comparison of Shading Strategies to Increase Human Thermal Comfort in Urban Areas. Atmosphere 9 (3), 91.
URL http://www.mdpi.com/2073-4433/9/3/91

Li, X., Stringer, L. C., Dallimer, M., 2022. The role of blue green infrastructure in the urban thermal environment across seasons and local climate zones in East Africa. Sustainable Cities and Society 80, 103798.
URL https://doi.org/10.1016/j.scs.2022.103798

Lindberg, F., Grimmond, C. S., Gabey, A., et al., 2018. Urban Multi-scale Environmental Predictor (UMEP): An integrated tool for city-based climate services. Environmental Modelling and Software 99, 70–87.

Manoli, G., Fatichi, S., Schläpfer, M., Yu, K., Crowther, T. W., Meili, N., Burlando, P., Katul, G. G., Bou-Zeid, E., 2019. Magnitude of urban heat islands largely explained by climate and population. Nature 573, 55–60.
URL http://dx.doi.org/10.1038/s41586-019-1512-9 https://www.nature.com/articles/s41586-019-1512-9

Martilli, A., Krayenhoff, E. S., Nazarian, N., 2020. Is the Urban Heat Island intensity relevant for heat mitigation studies? Urban Climate 31.
URL https://www.sciencedirect.com/science/article/pii/S2212095519300070

Masson, V., 2005. Urban surface modeling and the meso-scale impact of cities. Theoretical and Applied Climatology 84 (1-3), 35–45.
URL http://www.springerlink.com/index/10.1007/s00704-005-0142-3

Masson, V., Heldens, W., Bocher, E., Bonhomme, M., Bucher, B., Burmeister, C., Munck, C. D., Esch, T., Hidalgo, J., Kanani-Sühring, F., Kwok, Y.-T., Lemonsu, A., Lévy, J.-P., Maronga, B., Pavlik, D., Petit, G., See, L., Schoetter, R., Tornay, N., Votsis, A., Zeidler, J., 2020a. City-descriptive input data for urban climate models: Model requirements, data sources and challenges. Urban Climate 31, 100536.
URL https://doi.org/10.1016/j.uclim.2019.100536

Masson, V., Lemonsu, A., Hidalgo, J., Voogt, J., 2020b. Urban Climates and Climate Change. Annu. Rev. Environ. Resour., 411–444.

Middel, A., Krayenhoff, E. S., 2019. Micrometeorological determinants of pedestrian thermal exposure during record-breaking heat in Tempe, Arizona: Introducing the MaRTy observational platform. Science of the Total Environment 687, 137–151.
URL https://doi.org/10.1016/j.scitotenv.2019.06.085

Middel, A., Turner, V. K., Schneider, F. A., Zhang, Y., Stiller, M., 2020. Solar reflective pavements A policy panacea to heat mitigation? Environ. Res. Lett.

Nazarian, N., Sin, T., Norford, L., 2018. Urban Climate Numerical modeling of outdoor thermal comfort in 3D. Urban Climate 26, 212–230.

Nice, K. A., 2016. Development, validation, and demonstration of the VTUF-3D v1.0 urban micro-climate model to support assessments of urban vegetation influences on human thermal comfort. Phd thesis, Monash University.

Nice, K. A., Coutts, A. M., Tapper, N. J., 2018. Development of the VTUF-3D v1.0 urban micro-climate model to support assessment of urban vegetation influences on human thermal comfort. Urban Climate 24, 1052–1076.

Nicholls, N., Skinner, C., Loughnan, M., et al., 2008. A simple heat alert system for Melbourne, Australia. International Journal of Biometeorology 52 (5), 375–84.
URL http://www.ncbi.nlm.nih.gov/pubmed/18058138

Oke, T., 1982. The energetic basis of the urban heat island. Quarterly Journal of the Royal Meteorological Society 108, 1–24.
URL http://onlinelibrary.wiley.com/doi/10.1002/qj.49710845502/abstract

Oke, T. R., Mills, G., Christen, A., Voogt, J. A., 2017. Urban Climates. Cambridge University Press, Cambridge.

Ossola, A., Jenerette, G. D., McGrath, A., Chow, W., Hughes, L., Leishman, M. R., 2021. Small vegetated patches greatly reduce urban surface temperature during a summer heatwave in Adelaide, Australia. Landscape and Urban Planning 209, 104046.
URL https://doi.org/10.1016/j.landurbplan.2021.104046

pandas development team, T., Feb. 2020. pandas-dev/pandas: Pandas.
URL https://doi.org/10.5281/zenodo.3509134

Pebesma, E., 2018. Simple Features for R: Standardized Support for Spatial Vector Data. The R Journal 10, 439–446.

Pedregosa, F., Varoquaux, G., Gramfort, A., Michel, V., Thirion, B., Grisel, O., Blondel, M., Prettenhofer, P., Weiss, R., Dubourg, V., Vanderplas,

J., Passos, A., Cournapeau, D., Brucher, M., Perrot, M., Duchesnay, E., 2011. Scikit-learn: Machine learning in Python. Journal of Machine Learning Research 12, 2825–2830.

Peng, W., Wang, R., Duan, J., Gao, W., Fan, Z., 2022. Surface and canopy urban heat islands: Does urban morphology result in the spatiotemporal differences? Urban Climate 42, 101136.
URL https://doi.org/10.1016/j.uclim.2022.101136

Perkins-Kirkpatrick, S. E., Lewis, S. C., 2020. Increasing trends in regional heatwaves. Nature Communications 11 (3357).
URL http://dx.doi.org/10.1038/s41467-020-16970-7

Potgieter, J., Nazarian, N., Lipson, M. J., Hart, M. A., Ulpiani, G., Morrison, W., Benjamin, K., 2021. Combining High-Resolution Land Use Data With Crowdsourced Air Temperature to Investigate Intra-Urban Microclimate. Frontiers in Enviromental Science 9, 720323.

Solcerova, A., van Emmerik, T., Hilgersom, K., van de Ven, F., van de Giesen, N., 2018. Uchimizu: A Cool(ing) Tradition to Locally Decrease Air Temperature. Water 10 (741).

Stewart, I. D., Oke, T. R., 2012. Local Climate Zones for Urban Temperature Studies. Bulletin of the American Meteorological Society 93 (12), 1879–1900.
URL http://journals.ametsoc.org/doi/abs/10.1175/BAMS-D-11-00019.1

Stewart, I. D., Oke, T. R., Krayenhoff, E. S., 2014. Evaluation of the local climate zone' scheme using temperature observations and model simulations. International Journal of Climatology 34, 1062–1080.

Verdonck, M.-L., Demuzere, M., Hooyberghs, H., Beck, C., Cyrys, J., Schneider, A., Dewulf, R., Van Coillie, F., 2018. The potential of local climate zones maps as a heat stress assessment tool, supported by simulated air temperature data. Landscape and Urban Planning, 183–197.
URL https://doi.org/10.1016/j.landurbplan.2018.06.004

Wilke, C. O., 2020. ggridges: Ridgeline plots in 'ggplot2'. R package version 0.5.2.
URL https://CRAN.R-project.org/package=ggridges

Zhu, X., Liang, S., Pan, Y., 2012. Observational evidence of the cooling effect of agricultural irrigation in Jilin, China. Climatic Change 114, 799–811.

7. Acknowledgements

KAN is supported by NHMRC/UKRI grant (1194959).

8. Credit Author Statement

KAN: Conceptualization, Methodology, Software, Formal Analysis, Writing - Original Draft, Writing - Review & Editing, Visualization. **NN**: Methodology, Writing - Original Draft, Writing - Review & Editing. **MJL**: Methodology, Writing - Review & Editing. **MAH**: Methodology, Writing - Original Draft, Writing - Review & Editing. **SS**: Methodology, Writing - Review & Editing. **JT**: Writing - Review & Editing. **MN**: Data Curation. **BG**: Writing - Review & Editing. **MS**: Writing - Review & Editing.

9. Supplementary Figures

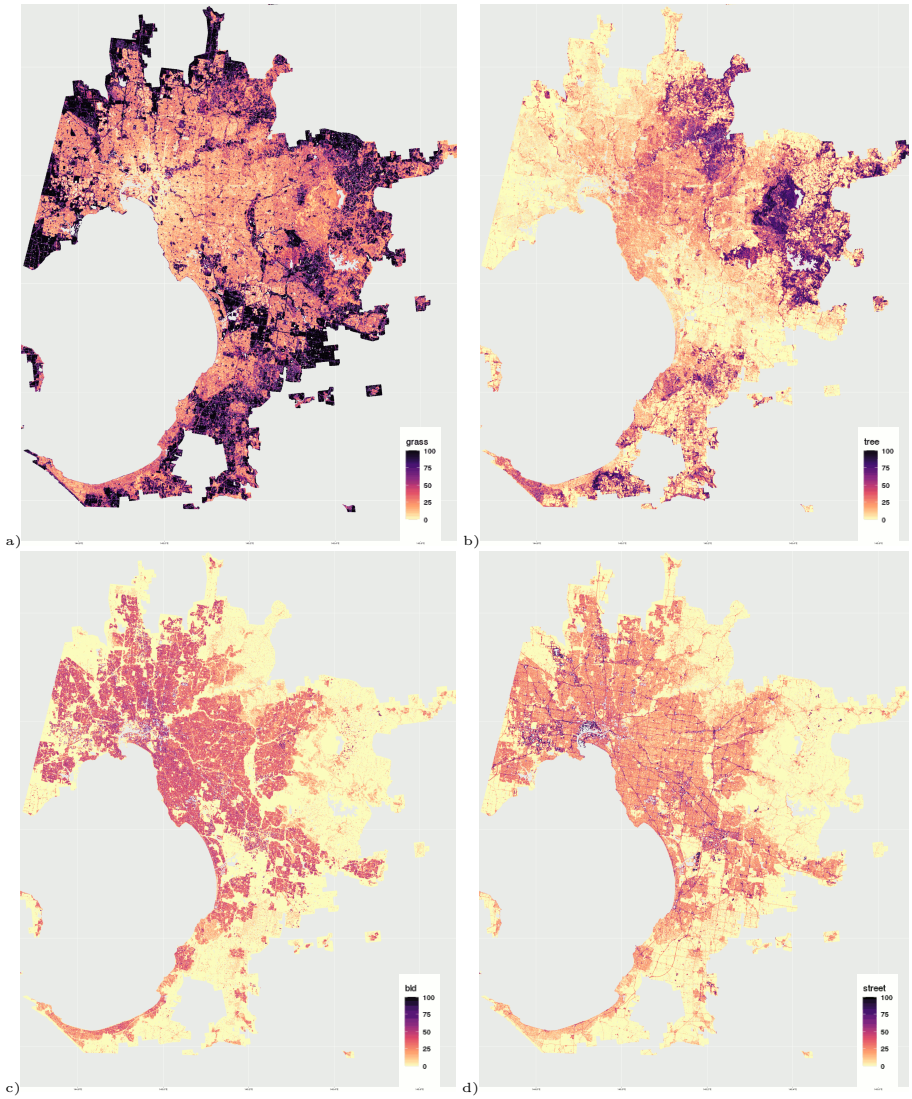

Figure S1: **Surface fractions of a) grass, b) trees, c) buildings, and d) streets across Melbourne.**

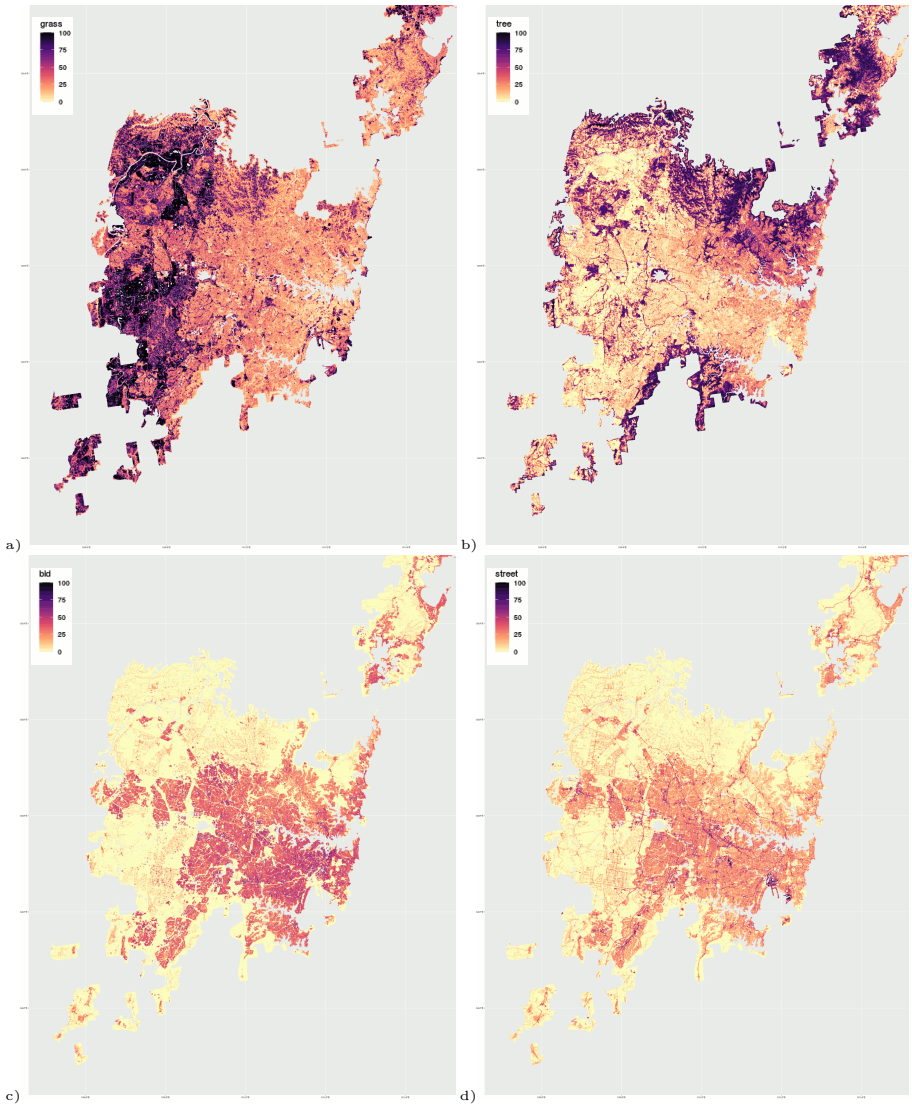

Figure S2: **Surface fractions of a) grass, b) trees, c) buildings, and d) streets across Sydney.**

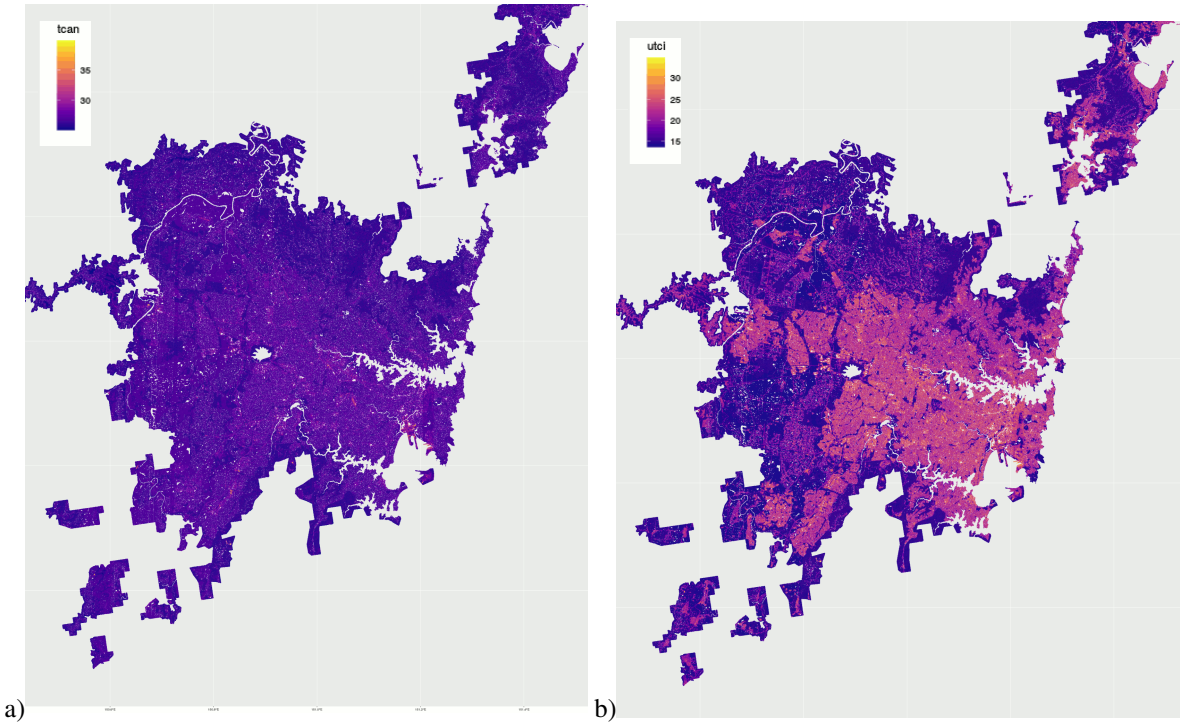

Figure S3: **a)** T_{can} **and b)** $UTCI$ **heatmaps on February 12, 2004 at 2pm generated by matching the closest matching parameters of surface fractions and average heights for each 100×100m location in Sydney from 9814 modelled scenario results (in** °C**).**

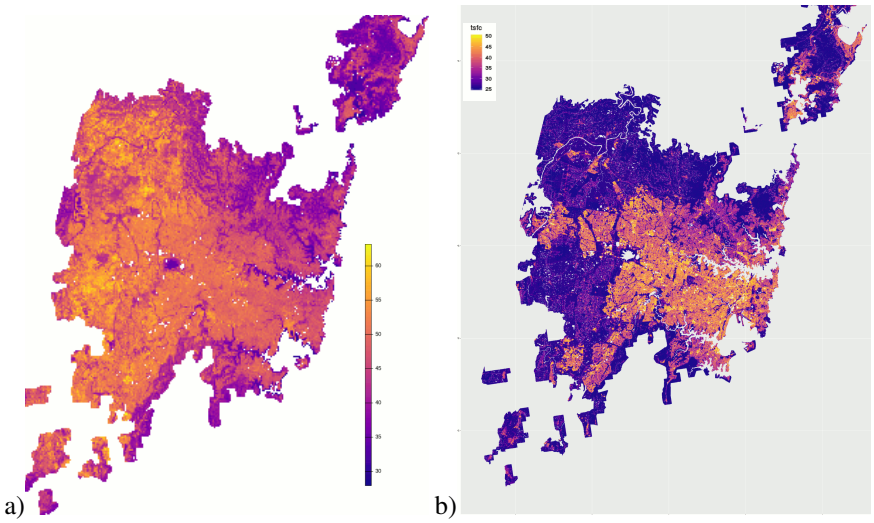

Figure S4: **a) Landsat 8 land surface temperature** (°C) **captured 10am March 11, 2019. Local conditions of air temperature on this day were minimum and maximum of 22 and 26**°C**. b) Modelled** T_{sfc} (°C) **on February 12, 2004 at 10am generated by matching the closest matching parameters of surface fractions and average heights for each 100×100m location in Sydney from 9814 modelled scenario results.**

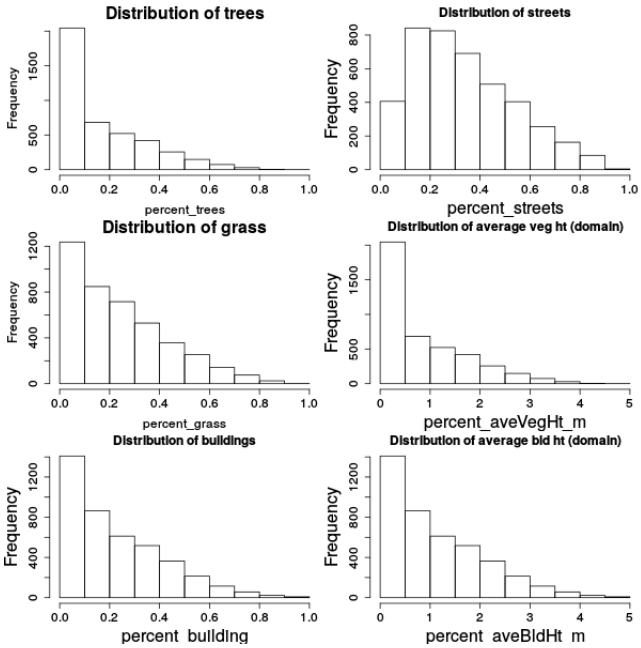

Figure S5: **Distribution of surface types across all modelled scenarios.**